Published in final edited form as:
Nat Chem Biol. 2015 March ; 11(3): 229–234. doi:10.1038/nchembio.1750.

Lipid vesicles trigger α-synuclein aggregation by stimulating primary nucleation

Céline Galvagnion[1], **Alexander K. Buell**[1], **Georg Meisl**[1], **Thomas C.T. Michaels**[1], **Michele Vendruscolo**[1], **Tuomas P.J. Knowles**[1], and **Christopher M. Dobson**[1]
[1]Department of Chemistry, University of Cambridge, Lensfield Road, Cambridge CB2 1EW, UK

Abstract

α-synuclein (α-syn) is a 140-residue intrinsically disordered protein that is involved in neuronal and synaptic vesicle plasticity but its aggregation to form amyloid fibrils is the hallmark of Parkinson's disease (PD). The interaction between α-syn and lipid surfaces is believed to be a key feature for mediation of its normal function but under other circumstances is able to modulate amyloid fibril formation. Using a combination of experimental and theoretical approaches, we have identified in this study the mechanism through which facile aggregation of α-syn is induced under conditions where it binds to a lipid bilayer, and we show that the rate of primary nucleation can be enhanced by three orders of magnitude or more under such conditions. These results reveal the key role that membrane interactions can play in triggering conversion of α-syn from its soluble state into the aggregated state that is associated with neurodegeneration and to its associated disease states.

Introduction

Substantial evidence links α-synuclein (α-syn), a small (14 kDa) highly conserved pre-synaptic protein, to both familial and sporadic types of Parkinson's disease 1–7. When isolated in solution, α-syn is intrinsically disordered but in the presence of lipid surfaces the protein adopts a highly helical structure 8–14 that is believed to mediate its normal functions, including control of synaptic membrane processes and biogenesis, regulation of neurotransmitter release and synaptic plasticity, and modulation of neuronal survival 2,6,15–19. The interaction between α-syn and lipids has also been shown to modulate amyloid fibril formation in different ways depending on the relative proportion of the two species 20–25. Recent studies have suggested that α-syn may co-aggregate with lipid molecules upon amyloid formation, and that the lipid:protein ratio can affect the morphology of the amyloid fibrils 26, indicating the importance of achieving a global understanding of the effect of lipids on the kinetics of amyloid formation by α-syn.

Correspondence: Correspondence and requests for materials should be addressed to C.M.D. (cmd44@cam.ac.uk).

Competing Interests: The authors declare they have no competing interests as defined by Nature Publishing Group, or other interests that might be perceived to influence the results and discussion reported in this paper.

Authors contributions: CG performed the experiments and AKB recorded the AFM images. CG, AKB, TPJK, MV and CMD were involved in the design of the study. CG, AKB, GM and CMD wrote the paper and all the authors were involved in the analysis of the data and editing of the paper.

Europe PMC Funders Author Manuscripts

In the study reported here, we identify by means of a combination of experimental and theoretical approaches a mechanism through which small unilamellar vesicles (SUVs) prepared from the phospholipid 1,2-dimyristoyl-sn-glycero-3-phospho-L-serine (DMPS) perturb the kinetics of α-syn amyloid formation 27–29. Our findings indicate that the presence of SUVs can enhance the rate of the essential primary nucleation step that initiates amyloid formation by three orders of magnitude or more, providing a global explanation of the dramatic modulation of the kinetics of α-syn amyloid formation by lipid vesicles 20,22,24,25. By contrast, under these conditions other microscopic processes, including homogeneous primary nucleation in bulk solution, secondary nucleation and fragmentation, do not contribute significantly to the aggregation reaction. These results provide a mechanistic description of the key role that specific membrane interactions can play in triggering conversion of α-syn from its soluble state into the aggregated state that is associated with neurodegenerative disease.

Results

The kinetics of α-syn aggregation are modulated by SUVs

In this study, we chose to work with a physiologically relevant lipid, phosphatidylserine (PS), which, together with phosphatidylcholine (PC) and phosphatidylethanolamine (PE), is one of the most abundant components of the membranes of synaptic vesicles 30. In order to probe the influence of lipid vesicles on the aggregation behaviour of α-syn, we first investigated the interaction between the protein and SUVs prepared from DMPS, using circular dichroism (CD) spectroscopy (Fig. 1a and Supplementary Results, Supplementary Fig. 1a). We monitored the change in the mean residue ellipticity of α-syn (25 μM (blue data) and 50 μM (black data)) for increasing DMPS:α-syn ratios, and the data are consistent with a single-step mode of binding (Fig. 1a) with a dissociation constant, K_D, of 3.8 ± 1.3 • 10^{-7} M and a stoichiometry, L, of 28.2 ± 0.8, where L is the total number of DMPS molecules in the bilayer that are involved in binding one molecule of α-syn. Interestingly, the size of the vesicles in the range of 20 - 100 nm does not detectably affect the affinity of the protein for the vesicles (See Supplementary Fig.1b). It is also interesting to note that if we assume that the lipid-bound protein molecules occupy a shell of 5 nm thickness on the external surfaces of the SUVs, by taking the hydrodynamic radius of the protein to be 26 Å 31 we can convert this stoichiometry into a local effective concentration of ca. 36 mM (See Methods for details), nearly 10^3 times higher than that in bulk solution. We then monitored the kinetics of aggregation of α-syn in the presence of these SUVs at 30°C under quiescent conditions, using different DMPS:α-syn ratios (Fig. 1b-d).

In the absence of SUVs under these conditions, no increase in the fluorescence signal of ThT was observed over more than 65 hours, indicating the absence of detectable amyloid formation 22. Similarly, no increases in ThT fluorescence were detected when α-syn (50 μM) was incubated in the presence of an excess of DMPS SUVs (DMPS:α-syn > 40), i.e. when the only state of the protein that is significantly populated is that bound to the SUVs (Fig. 1a); this finding is consistent with, and indeed rationalises, previous conclusions that the presence of lipid vesicles can inhibit amyloid formation by α-syn 24,25,32. In addition, however, when short pre-formed fibrils (20 μM) were incubated with an excess of DMPS

SUVs (2, 4 and 8 mM, DMPS:α-syn > 100), the protein was found to dissociate from the fibrils (Fig. 2a) and to populate the lipid-bound monomeric α-helical state (Fig. 2b) (See Methods for details). This transition is most likely to occur via the dissociation from the fibrils of monomeric α-syn, which, once free in solution, can bind to the SUVs; indeed the slow time scale of the equilibration, ca. 3 hours (Fig. 2a), is consistent with this mechanism (See Methods for details). This observation, together with the K_D value measured for the interaction between α-syn and SUVs, indicates that the lipid-bound α-helical state of α-syn is thermodynamically more stable than the fibrillar state under these conditions. Therefore, the absence of amyloid formation in the presence of high concentrations of SUVs, as well as the dissolution of pre-formed fibrils, can easily be rationalised as two manifestations of the high thermodynamic stability of the lipid-bound state.

By contrast, when α-syn (50 μM) was incubated at lower concentrations of DMPS (DMPS:α-syn ratios between 2 and 15), i.e., when there were significant populations of monomer both free in solution and bound to the vesicles, rapid formation of amyloid fibrils was observed independently of the average size of the vesicles (See Supplementary Fig 2), the quantities of which increased steadily as the concentration of DMPS was increased (Fig. 1b). In addition, as the DMPS:α-syn ratio was increased, the rate of amyloid formation decreased (Fig. 1b-d), a finding that can be attributed to the depletion of free monomeric α-syn in solution by the presence of DMPS SUVs; a similar phenomenon has been observed for the Aβ-peptide, the aggregation of which is associated with Alzheimer's disease, in the presence of polymeric nanoparticles 33. This observed decrease of the rate of amyloid formation for high DMPS:α-syn ratios is also likely to be attributable in part to an increasing average distance between the molecules of α-syn bound to the SUVs, thus reducing its local concentration. Taken together, these results show that the maximum rate of amyloid formation by α–syn in the presence of DMPS SUVs is observed for DMPS:α-syn ratios of 8; below this value, the rate of amyloid formation is limited by the concentration of bound α-syn, whereas above this value the rate of aggregation is limited by the concentration of free monomeric protein.

We compared the binding of α-syn to DMPS SUVs in the absence and presence of added salt (sodium chloride, NaCl, at concentrations of 25 and 50 mM). The affinity of α-syn for the DMPS SUVs was observed to decrease as the concentration of NaCl increased, (Fig. 3a) as illustrated by the increase in both the stoichiometry (from ca. 28 (no salt) to ca. 60 (50 mM NaCl)) and the dissociation constant (from 0.38 (no salt) to 11 μM (50 mM NaCl)) upon addition of NaCl; this observation is attributable to the screening of the electrostatic interactions between the negatively charged lipid polar heads of the SUVs and the positively charged N-terminal region of α-syn. We then monitored the formation of amyloid fibrils in the absence and the presence of 25 and of 50 mM NaCl (Fig. 3b) and observed that the kinetics of amyloid formation slowed down as the concentration of NaCl increased, suggesting that the interaction between α-syn and the DMPS SUVs is necessary to stimulate α-syn aggregation. Overall, these results reveal that the presence of SUVs very strongly enhances the rate of amyloid formation by α-syn under the conditions used here where the DMPS:α-syn ratio is lower than 40 (Fig. 1c), i.e. when there is free as well as bound α-syn present in solution as we discuss further below.

α–syn and SUVs play distinct roles in amyloid formation

The experimental data show, therefore, that there is a dynamical equilibrium between the protein free in solution and bound to vesicles. In order to understand the contribution of these two populations (free and bound α-syn) to the kinetics of amyloid formation, we monitored the formation of amyloid fibrils under conditions where the concentrations of α-syn free in solution (Fig. 4a) and bound to the vesicles (Fig. 4b) were systematically varied in turn by changing the total concentrations of both protein and DMPS SUVs (Eqs. 6-8 in Methods). The concentration of protein molecules converted into fibrils, determined by absorbance analysis (Eqs. 9 and 10 in Methods), was found to be constant, at ca.15 μM, when the concentration of DMPS was 300 μM, for all the different initial concentrations of α-syn free in solution (Fig. 4c); it was, however, found to be proportional to the initial concentration of α-syn bound to the vesicles, with a constant of proportionality of approximately two (Fig. 4d). Interestingly, if secondary processes such as fibril fragmentation or autocatalytic nucleation 27 were to contribute to the formation of new fibrils, the total concentration of protein converted into fibrils would be expected to approach the initial concentration of free monomeric protein (see Fig. 4c,d). Our results reveal, however, that under the conditions used here, the concentration of protein converted into fibrils when the aggregation kinetics had reached the plateau phase (Fig. 4a,b) did not depend on the initial concentration of free α-syn but rather on that of DMPS (Fig. 4c,d).

In order to probe whether or not the nucleation and growth of amyloid fibrils on the lipid vesicles influences the structure of the SUVs, we used membrane fluidity as observable by monitoring changes in fluorescence polarisation (FP) of 1,6-diphenylhexa-1,3,5-triene (DPH) 34. Interestingly, the binding of monomeric α-syn to the DMPS membrane decreased its melting temperature from 41°C to 30°C (Supplementary Fig. 3a); a similar finding has been reported for DPPC membranes 35. In addition, the fluorescence polarisation of DPH when embedded within the membrane bilayers was observed to be enhanced as amyloid formation proceeded (Supplementary Fig. 3b), suggesting that the bilayer becomes even more rigid 34 and that the formation of amyloid fibrils does not disrupt the lipid vesicles.

Analysis using atomic force microscopy (AFM) indicated that two distinct types of structures were present in the plateau region of ThT fluorescence (Fig. 5a,b), both of which differ from those observed in the absence of SUVs (Fig. 5c) 36. Some structures appear as small spherical species with a diameter of < 50 nm, and can be attributed to SUVs coated with α-syn molecules, and other species can be identified as thin (< 5 nm in height) filaments that appear to be attached to the SUVs, and we attribute these species to amyloid fibrils whose formation had been nucleated on the surface of the SUVs. The average length of the fibrils observed by AFM is ca. 375 nm, a value indicating that on average only a single nucleation event had occurred at each vesicle (see Methods for details). This observation, along with the images from the AFM analysis, shows that only a small fraction of all bound α-syn molecules contributes to the formation of an active nucleus from which a fibril can grow.

These experiments also indicate that a large proportion of monomeric protein molecules remained in solution when no further change in the ThT fluorescence intensity was observed (Fig. 4c), showing that amyloid formation induced by the presence of SUVs had slowed

down and effectively ceased by mechanisms other than that of the simple depletion of free monomer that is generally observed during studies of amyloid formation in homogeneous solution 37. Indeed, we isolated the remaining free monomer at the end of the first amyloid formation reaction (See Methods for details) and incubated the latter with a fresh solution of DMPS SUVs (Fig. 5d); this incubation resulted in a second batch of fibrils with morphologies very similar to those of the species formed in the initial reaction (Fig. 5d). Furthermore, sonication of the reaction mixture resulted in the breakage of fibrils into small fragments (Fig. 5e) that with further incubation grew into much larger fibrils with a morphology very similar to that of fibrils formed in the absence of lipid vesicles in an agitated solution (Fig. 5e) 36. These findings suggest that the end state of the aggregating solution, i.e. when the plateau in fluorescence intensity is reached, represents a kinetically trapped state due to the quiescent conditions used in these experiments. Under other conditions the fibrils would be able to proliferate as a result of secondary processes such as fragmentation as we show using sonication techniques. These conditions thus allow us to probe in detail the primary nucleation process that is otherwise difficult to study because, in the presence of secondary processes, the latter usually dominate the kinetics of the aggregation reaction 38.

Taken together, therefore, these observations show that the rates of secondary nucleation and fragmentation are negligible under the quiescent conditions of our experiments, and that amyloid formation ceases either because of the depletion of nucleation sites on the SUVs and/or because of the inactivation of growing fibril ends, and not because of the depletion of free α-syn. These results therefore indicate that the effect of the SUVs is to enhance dramatically the rate of primary nucleation of α-syn self-assembly.

Vesicles can enhance the nucleation rate by a thousand-fold

Analysis of the kinetics of amyloid formation under carefully chosen and controlled conditions has been shown to enable the determination of the key microscopic steps in the mechanism of protein aggregation as well as their associated molecular rate constants 27–29,39–42. Substantial evidence points towards the fact that heterogeneous primary nucleation, i.e. nucleation taking place at an interface, for example air/water or lipid/water, rather than homogeneous primary nucleation involving only free monomers in bulk solution, is the initial step in α-syn aggregation 43–45. We considered two possible mechanisms to describe the heterogeneous primary nucleation process accelerated by the presence of SUVs. The first and simplest is a ”one-step nucleation” model, directly converting monomers into nuclei 46 (Eqs. 11-13 in Methods). In addition, we considered a more complex mechanism involving a conversion step in the nucleation process; indeed, a conversion step has been found from single molecule experiments 47 to occur during the formation of α-syn aggregates in bulk solution under shear conditions, where initially formed disorganised oligomers were found to convert into more highly structured species. In this ”two-step nucleation” model, a pre-nucleus, (indicated as A in the kinetic equations in the Methods) is formed and then rearranges, with a rate constant k_b, to form a growth competent nucleus, P (Eqs. 11 and 14-17 in Methods). In the analysis, we have focused on the early times of the aggregation reaction where the influence of primary nucleation is most marked. Moreover, in this regime, the concentration of monomeric protein remains constant to a good

approximation, a factor that allows an analytical treatment of the rate equations 39,48. Using this approach, we found that both models of nucleation can describe well the early time regions of the complete set of experimental curves (Fig. 6a,b and Supplementary Fig. 4) where our analysis is applicable (see Methods), confirming that a greatly enhanced primary nucleation rate is the origin of the much more rapid formation of amyloid fibrils in the presence of SUVs.

Global analysis of the kinetic data, in which all the aggregation time courses in a series of experiments are fitted with a single set of parameters, also indicates that the apparent reaction order of the nucleation step relative to free monomeric protein is ca. 0.2, i.e. it is close to 0, whilst homogeneous primary nucleation rates in bulk solution typically have reaction orders greater than 1.0 37. This observation reveals that the formation of α-syn nuclei in the presence of vesicles does not depend significantly on the concentration of free monomer, and therefore that free monomers are not directly involved in the rate-determining step of the nucleation process.

This analysis shows in addition that the rate of fibril elongation from the vesicles saturates at monomer concentrations higher than ca. 100 μM, a value close to that observed for the saturation of the elongation of pre-formed fibrils in the absence of SUVs 36. If we make the assumption that the elongation rate constant is similar in the presence of SUVs to that in their absence, the latter having been determined to be ca. $2 \cdot 10^3$ M^{-1} s^{-1} 36, the rate of formation of new nuclei by α-syn at the membrane interface can be estimated from our analysis to be ca. $1 \cdot 10^{-14}$ M s^{-1} at a DMPS concentration of 300 μM. This value is, remarkable, more than three orders of magnitude greater than the upper limit of the nucleation rate estimated for quiescent conditions in the absence of SUVs ($7 \cdot 10^{-18}$ M s^{-1}, see Methods for details). Interestingly, an analysis using the ”two-step nucleation” model requires a rate of conversion between the two types of nuclei of ca. $2 \cdot 10^{-5}$ s^{-1}. This rate is very close to the rate of conversion between the two distinct types of oligomers observed in single molecule experiments, $5 \cdot 10^{-6}$ s^{-1}, in the absence of SUVs 47, suggesting that this two-step model could well apply to the type of heterogeneous nucleation in the presence of SUVs that has been identified in the present work (see residuals of the fits using the two models in Supplementary Fig. 5).

Discussion

The results described in this paper provide a self-consistent explanation for the observed modulation of α-syn amyloid formation by lipid vesicles 20,22. At high lipid:α-syn ratios, essentially all of the protein molecules are bound to the surface of the vesicles, in predominantly helical conformations 10, and, in the absence of free monomeric α-syn, aggregation does not take place at a detectable rate. At low lipid:α-syn ratios, however, when free monomer is present in solution, primary nucleation occurs on the vesicle surfaces on which α-syn is bound. The rate of this nucleation reaction is at least three orders of magnitude greater than that occurring in bulk solution, a result that can be attributed to the high local concentration of protein molecules at the surface of the vesicle and to their likely ability to explore conformations that may favour primary nucleation but are rare in solution

10. It is important to note in this context that the magnitude by which the rate of primary nucleation rate is increased by lipid vesicles is likely to be affected by their composition.

Interestingly, it has recently been shown that the numbers of vesicles and of α-syn molecules in a functional synaptosome, or synaptic button, are ca. 400 and ca. 3000, respectively, which correspond to an α-syn:vesicle ratio of ca. 10:1 49. In our study, we have shown that lipid vesicles enhance amyloid fibril formation when the DMPS:α-syn is below 40, corresponding to a α-syn:vesicle ratio of 100:1, a value one order of magnitude greater than that observed in vivo. Given the difference between the composition of DMPS SUVs and synaptic vesicles, however, it is noteworthy that these ratios are similar to within an order of magnitude. In addition, the fact that we have observed a closely similar enhancement of the primary nucleation rate of α-syn in the presence of both small (SUVs, < 20nm diameter) and large DMPS (LUVs, > 100nm diameter) vesicles suggests that membrane curvature does not play a very significant role for either the binding or the nucleation of α-syn, at least under the conditions used in our study, presumably because even the smallest vesicles are not significantly curved on the scale of a protein monomer, enabling us to state that our results are significant in the context of the vesicle sizes found in vivo, e.g. the secretory vesicles for neurotransmitters have a diameter of ca. 40 nm 49.

The fact that the stimulation of amyloid formation via the enhancement of primary nucleation, the vital first step in any spontaneous aggregation process, occurs only above a threshold value of the α-syn:lipid ratio is of particular interest in the light of evidence that over-expression of α-syn via gene duplication or triplication, both of which are likely to lead to an increase in the α-syn:synaptic vesicle ratio in vivo, results in early onset forms of Parkinson's disease 19. Such changes reflect the fact that the transition between functional interactions of α-syn with lipid membranes and deleterious ones that can generate pathogenicity is likely to be finely balanced, such that relatively small changes in concentration can cause dramatic increases in the risk of pathogenic behaviour 50. The present findings, therefore, contribute to our understanding of how the aggregation of α-syn in vivo can lead not only to a lack of functional protein molecules but also to species toxic to neuronal cells in vivo 2. More generally, the discovery of the dramatic increase that can occur in the rate of the primary nucleation of α-syn in the presence of specific membrane surfaces provides a possible explanation of the way that the key initial steps in the process of aggregation of α-syn could occur in a cellular environment and ultimately lead to the onset and proliferation of disease.

Online methods

Reagents

1,2-dimyristoyl-*sn*-glycero-3-phospho-L-serine (sodium salt) (DMPS) was purchased from Avanti Polar Lipids, Inc. Sodium phosphate monobasic (NaH_2PO_4, BioPerformance Certified, ≥ 99.0%), sodium phosphate dibasic (Na_2HPO_4, ReagentPlus®, ≥ 99.0%), sodium chloride (NaCl, BioXtra ≥ 99.5%), 1,6-diphenylhexa-1,3,5-triene (DPH, 98%), ethanol (EtOH, ≥ 99.8%) and Triton X-100 were purchased from Sigma Aldrich. Thioflavin T UltraPure Grade (ThT, ≥ 95%) was purchased from EUROGENTEC LTD.

Europe PMC Funders Author Manuscripts

Protein and lipid preparation

Wild type α-syn was expressed and purified as previously described 36,51. The lipids were dissolved in 20 mM phosphate buffer (NaH_2PO_4/NaH_2PO_4), pH 6.5, and stirred at 45°C for two hours. The solution was then frozen and thawed 5 times using dry ice and a water bath at 45°C, respectively. The preparation of small or large unilamellar vesicles, SUVs or LUVs, respectively, was done using sonication (3 × 5 min, 50 % cycles, 10 % maximum power) on ice or extrusion through 100 nm pore diameter membranes (Avanti Polar Lipids, Inc) at 45°C, respectively. After centrifugation, the sizes of the SUVs and LUVs were checked using dynamic light scattering (Zetasizer Nano ZSP, Malvern Instruments, Malvern, UK) and show to consist of a distribution centred at 20 and 100 nm diameter, respectively.

CD spectroscopy

Sample preparation and data acquisition—CD samples were prepared by incubating 50 μM α-syn in the presence of increasing concentrations of DMPS SUVs in 20 mM phosphate buffer, pH 6.5. Far-UV CD spectra were recorded on a JASCO J-810 equipped with a Peltier thermally controlled cuvette holder at 30°C. Quartz cuvettes with path lengths of 1 mm were used and CD spectra were obtained by averaging five individual spectra recorded between 250 and 200 nm with a bandwith of 1 nm, a data pitch of 0.2 nm, a scanning speed of 50 nm/min, and a response time of 1 s. Each value of the CD signal intensity reported at 222 nm corresponds to the average of five measurements, each acquired for 10 s. For each protein sample, the CD signal of the buffer used to solubilise the protein was recorded and subtracted from the CD signal of the protein.

Data analysis—The CD signal shown in this paper (CD_{obs}) can be described as follow:

$$CD_{obs} = x_B CD_B + x_F CD_F \quad (1)$$

where x_B and x_F are the fractions of α-syn bound to the membrane and free in solution, respectively, and CD_B and CD_F are the CD signals of the bound and free form of α-syn, respectively. By assuming that $x_B + x_F = 1$, and that the signals of α-syn in the presence of buffer, or in the presence of SUVs under saturating conditions, correspond to CD_F and CD_B, respectively, the fraction of α-syn bound to the SUVs for each sample can be expressed as:

$$x_B = \frac{CD_{obs} - CD_F}{CD_B - CD_F} \quad (2)$$

We use the following model: $F + DMPS_L \rightleftharpoons B(DMPS)_L$ and the corresponding equations (Eq. 2 and 6) to fit the data, where F and B are α-syn free in solution and bound to the vesicles, respectively, and L is the number of DMPS molecules interacting with one molecule of α-syn.

$$K_D = \frac{[F]\,[DMPS_L]}{\left[B(DMPS)_L\right]} \quad (3)$$

$$[\alpha - syn] = [F] + \left[B(DMPS)_L\right] \quad (4)$$

$$[DMPS] = L\left([DMPS_L] + [B\,(DMPS_L)]\right) \quad (5)$$

$$x_B = \frac{\left(\left([\alpha - syn] + \frac{[DMPS]}{L} + K_D\right) - \sqrt{\left(\left([\alpha - syn] + \frac{[DMPS]}{L} + K_D\right)^2 - \frac{4[DMPS][\alpha - syn]}{L}\right)}\right)}{(2\,[\alpha - syn])}$$

(6)

Using the values of K_D (in M), as well as the stoichiometry, L, obtained from the fit, we estimated the concentration of the protein bound to the vesicles (b) and of the protein free in solution (m) and for any given DMPS:α-syn ratio:

$$b = x_B\,[\alpha - syn] \quad (7)$$

$$m = [\alpha - syn] - b \quad (8)$$

Estimation of the local concentration of α-syn at the surface of a SUV

We estimated the local concentration of α-syn at the surface of each SUV by assuming that all the protein molecules bound to the lipid surface occupy a shell of 5 nm thickness at the outside of the SUVs, based on the hydrodynamic radius of monomeric α-syn in solution of 2.5 nm 31. This layer has a volume of $1.4 \cdot 10^{-24}$ m^3 $\left(V = \frac{4}{3}\pi r_1^3 - \frac{4}{3}\pi r_2^3, r_1 = 15\text{ nm and } r_2 = 10\text{ nm}\right)$. By assuming that the area per lipid of DMPS is of the order of 0.40 nm^2 52, we estimated that ~ 3,140 lipid molecules of DMPS are exposed per SUV $\left(\text{number of lipid exposed per vesicle} = \frac{\text{number of SUV}}{\text{surface per lipid of DMPS}}\right)$, therefore there are a total number of ~ 6,000 lipid molecules of DMPS per SUV. For a given

stoichiometry, L, the local concentration of α-syn at the surface of each SUV can be estimated by $[\alpha-\mathrm{syn}]_{\mathrm{local}} \sim \frac{6000}{\mathrm{L}\mathrm{N}_{\mathrm{A}}\mathrm{V}}$, with N_A the Avogadro number and V in dm^3.

Analysis of the dissociation of pre-formed α-syn amyloid fibrils by high concentrations of SUVs

The combined circular dichroism and ThT experiments shown in Figure 2 suggest that, even in the presence of 2 mM SUVs, 20 μM of pre-formed short (through sonication) fibrils are quantitatively dissociated. We can use the ThT time traces to analyse the kinetics of dissociation and check whether or not they are consistent with the dissociation of monomers from the ends of the fibrils, which subsequently bind to the SUVs. Therefore free monomers are constantly removed and the equilibrium is slowly shifted away from the fibrillar state. In principle, one would expect a constant rate of decrease of ThT fluorescence, if a homogeneous population of fibrils dissociates, as each fibril will dissociate independently of the others. We observe, however, that the rate of dissociation decreases over time. This feature presumably stems from the fact that the fibrils are not mono-dispersed in length, but rather display a distribution of lengths, ranging from less than 50 nm to more than 200 nm in length 36. Therefore the short fibrils will vanish first and the total number of dissociating fibrils will decrease with time, rationalizing the observed decrease in rate. For our analysis, we considered only the initial linear part of the data, where the concentration (by number) of fibrils is likely to correspond to the (known) initially added concentration.

The difference in absolute fluorescence intensity between the data in the presence of 2, 4 and 8 mM SUVs, as well as the small increase in fluorescence at the beginning of the experiments are likely to be due to effects of the lipids on the ThT fluorescence. If the curves are normalised such that the maximal values are set to 1.0 in each case, the initial rates of dissociation differ by less than a factor of two. We will use the mean of the three observed dissociation rates, $3.53 \cdot 10^{-9}$ M s^{-1} for our calculation of the molecular rate constant. The concentration by number of dissociating fibrils can be calculated from the average number of monomers per fibril (180 36) to be ca. $1.1 \cdot 10^{-7}$ M. Therefore we obtain a dissociation rate constant k_{off} of $3.2 \cdot 10^{-2}$ s^{-1}. This value can be compared to that of the dissociation rate constant that can be calculated by assuming that at thermodynamic equilibrium, the growth and dissociation rates are equal. The monomer concentration at equilibrium has been reported to be ca. 1.6 μM 53. Together with an elongation rate constant of $2.2 \cdot 10^{3}$ M^{-1} s^{-1} 36, this value yields a dissociation rate constant k_{off} of $3.52 \cdot 10^{-3}$ s^{-1}. The results of these two approaches give values that are consistent to within one order of magnitude and indeed the apparent difference may be due to the approximations made during the calculations, as well as to uncertainties in the reported values of the equilibrium free monomer concentration and the elongation rate constant. We conclude that the dissolution of the pre-formed fibrils upon the addition of excess concentrations of SUVs is consistent with a mechanism in which the SUVs bind most of the free monomeric α-syn molecules, which leads to a shift in the equilibrium distribution of species and leads to the slow disappearance of the fibrils. It is worth noting that, in this fibril dissolution experiment, both the initial and final fluorescence intensities depend on the lipid concentration, which can be attributed to a direct ThT-lipid interaction.

Europe PMC Funders Author Manuscripts

Fluorescence polarisation measurements

A stock solution of 2 mM DPH was prepared by solubilizing it in 100% EtOH overnight under stirring conditions at room temperature. The dye was then diluted into a stock solution of DMPS SUVs and the mixture was incubated at 45°C for 30 min; the final EtOH content of this mixture was kept below 0.5%. After incubation, the size of the SUVs was checked using dynamic light scattering (Malvern Instruments, Malvern, UK) and consisted of a distribution centred at a diameter of 23 nm. The DMPS SUVs embedded with DPH were then incubated in the absence and the presence of α-syn or 10% Triton X-100 and the different solutions were placed in Corning 96 well plates with half-area (black/clear bottom polystyrene) non-binding surfaces. The fluorescence polarisation of DPH was then monitored using a plate reader (Polarstar Omega, BMG Labtech, Aylesbury, UK) under quiescent conditions at temperatures ranging from 10 to 60°C. A 355 nm excitation filter and two matched emission filters (430 nm) were installed in the corresponding filter wheels.

Aggregation kinetics

Sample preparation and data acquisition—α-syn was incubated in 20 mM sodium phosphate, pH 6.5, in the presence of 50 μM of ultrapure ThT and increasing concentrations of DMPS SUVs. The change in the ThT fluorescence signal with time was monitored using a plate reader (BMG Labtech, Aylesbury, UK) under quiescent conditions at 30°C. Corning 96 well plates with half-area (black/clear bottom polystyrene) non-binding surfaces, were used for each experiment. We also used polystyrene binding plates and obtained the same kinetics of amyloid formation by α–syn in the presence of DMPS SUVs as those measured using non-binding plates. At the end of each aggregation experiment, the samples were ultracentrifuged at 90 krpm for 30 min and the concentration of the free monomer was calculated by measuring the UV spectrum of the supernatant and using the following expressions:

$$[\mathrm{ThT}] = \frac{\mathrm{Abs}_{410}}{\epsilon_{\mathrm{ThT},410}} \quad (9)$$

$$[\alpha - \mathrm{syn}]_{\mathrm{monomer}} = \frac{\mathrm{Abs}_{275} - [\mathrm{ThT}]\,\epsilon_{\mathrm{ThT},275}}{\epsilon_{\alpha-\mathrm{syn},275}} \quad (10)$$

where Abs_{275} and Abs_{410} are the absorbance values measured at 275 and 410 nm, respectively, $\varepsilon_{\mathrm{ThT,\,275}}$, $\varepsilon_{\mathrm{ThT,\,410}}$, $\varepsilon_{\alpha\text{-syn,\,275}}$, are the extinction coefficients of ThT at 275 and 410 nm and α-syn at 275 nm, whose values were taken as 3, 200, 22, 725 and 5, 600 M^{-1} cm^{-1} 54, respectively. The extinction coefficients of ThT at 275 nm and 410 nm were determined using a standard curve made by monitoring the absorbance spectra (250 - 600nm) of ThT samples whose concentration ranged from 0 to 50 μM. The concentration of the fibrils was then estimated using the following relationship: $[\alpha - \mathrm{syn}]_{\mathrm{fibrils}} = [\alpha - \mathrm{syn}]_{\mathrm{initial}} - [\alpha - \mathrm{syn}]_{\mathrm{monomer}}$, where $[\alpha - \mathrm{syn}]_{\mathrm{initial}}$ is the concentration of α-syn at t = 0 in the well.

Kinetic data analysis—The general approach to modelling the kinetics of fibrillar aggregation, as outlined previously 28,29, derives differential equations for the number P(t) and mass concentration M(t) of fibrils, which can then be solved to give the time evolution of the aggregation reaction. The processes usually taken into account are primary nucleation followed by elongation through addition of monomers to the fibril ends. In some systems secondary processes (i.e. formation of new growth-competent aggregates from existing aggregates, including fragmentation and heterogeneous nucleation on the surface of existing aggregates) are also relevant 37, but they were found to be negligible in the early time courses of the reactions studied in this work. In previous studies it has been shown that the elongation rate may saturate at high concentrations of monomeric α-syn 36, which we take account of by treating elongation as a Michaelis-Menten like process 55. The resulting differential equation for the formation of fibril mass, M(t), is given by:

$$\frac{dM}{dt} = k_+ \frac{m(t)}{1 + \frac{m(t)}{K_M}} P(t) \qquad (11)$$

where k_+ is the elongation rate constant, m(t) is the free monomer concentration, P(t) is the number concentration of fibrils and K_M is the Michaelis constant, which gives the monomer concentration at which saturation effects become important55. We then consider two different possible nucleation mechanisms, to obtain the equations for the variation in fibril numbers:

Single-step nucleation:

The simplest model is a nucleated growth model 46. As the present system involves nucleation only at the surface of vesicles (heterogeneous primary nucleation), we assume that the rate of heterogeneous primary nucleation also depends on the concentration, ”b”, of bound α-syn. The corresponding differential equation is given by:

$$\frac{dP}{dt} = k_n b m(t)^n \qquad (12)$$

where k_n is the heterogeneous primary nucleation rate constant and n is the reaction order of the heterogeneous primary nucleation reaction relative to the free monomer, m(t). Note that for systems with a constant concentration of bound α-syn this process is equivalent to simple homogeneous nucleation in solution with an effective rate constant of $k_n b$. It is clear that the concentration of ”active” bound α-syn, i.e. bound α-syn that is able to form nuclei, will decrease over the course of a reaction, as free monomer remains at the plateau phase of the reaction and therefore heterogeneous nucleation processes must have ceased to produce new growth-competent nuclei. In the present study, we focus on the early time points in the overall reaction, when this effect is unlikely to play any significant role. In the early time limit, we can set m(t) = m(0), which is equivalent to assuming that the depletion of monomer is insignificant for early times. Equations 11 and 12 can easily be solved and yield for the case of an unseeded reaction:

$$M(t) = \frac{K_M k_+ m(0)^{n+1} k_n b t^2}{2(K_M + m(0))} \quad (13)$$

Note the characteristic t^2 dependence that arises from this expression.

Two-step nucleation:

At the next stage of complexity we introduce one conversion step into the heterogeneous primary nucleation process: the first step of the productive nucleation process is the formation a pre-nucleus, A, which then rearranges with rate constant k_b to form a growth competent nucleus. The relevant equations are:

$$\frac{dA}{dt} = K_n b m(t)^n - k_b A(t) \quad (14)$$

$$\frac{dP}{dt} = K_b A(t) \quad (15)$$

As before, the solutions for the early time limit can easily be derived, yielding:

$$M(t) = \frac{k_M k_n m(0)^{n+1} b}{k_b^2 (K_M + m(0))} \left(-k_+ (e^{-k_b t} - 1) + \frac{k_+ k_b^2 t^2}{2} - k_b k_+ t\right) \quad (16)$$

Expansion of the exponential for the short time gives a t^3 leading term (Eq. 17), predicting a sharper increase in aggregate concentration in the two-step nucleation mechanism than that predicted in the single-step nucleation mechanism.

$$M(t) = \frac{K_M k_n m(0)^{n+1} b k_b k_+ t^3}{6(K_M + m(0))} \quad (17)$$

We note that in the regime where we observe stimulation of α-syn aggregation by SUVs, the local concentration of the protein at the surface of the vesicles is essentially constant. In fact, a change in lipid concentration leads only to a change in the total macroscopic concentration of bound protein, and not to a change in the local concentration of the protein at the surface of each vesicle. Therefore, the reaction order of the nucleation step with respect to bound protein is not accessible through our current experimental strategy. An increase in lipid concentration will indeed lead to a proportional increase in nucleation rate, simply due to the fact that there is a larger lipid surface for the nucleation to take place on.

Fitting of the kinetic data—The above early time solutions (Eqs. 13 and 16) were used to fit globally the first 30 h of the kinetic traces at all the monomer and lipid concentrations shown in Fig. 6 and Supplementary Fig. 4. The fits were performed using the Knowles group online aggregation fitter (http://www.amylofit.ch.cam.ac.uk/), which is based on a basin-hopping algorithm 56. The residuals are the difference between the fitted curves and the experimental values (average this over the repeats), at each data point (Supplementary Fig. 5). The mean squared error of the fits (as indicated in the legends of Supplementary Fig. 5) is the sum of all squared residuals over the number of data points minus the number of free parameters i.e.

$$\text{Residuals}=\frac{\sum_{i}^{N}(f(x_i)-y_i)^2}{N-N_p} \quad (18)$$

where N is the number of data points and N_p is the number of free parameters.

Comparison of the rate of formation of new nuclei via primary nucleation of α-syn under quiescent conditions in the presence and absence of SUVs

Quiescent conditions in the absence of SUVs—In order to compare the rate of formation of new nuclei via primary nucleation of α-syn under quiescent conditions in the presence and absence of SUVs, we first estimated the upper bound of this rate in the absence of SUVs. We have recently shown that under quiescent conditions and in the absence of SUVs, the rate of secondary nucleation is negligible at pH values above 6 36. Our data shows in fact that in the absence of SUVs, no fibrils are detected when 140 μM α-syn is incubated under quiescent conditions during 125h (Supplementary Fig. 6) suggesting that the rate of primary nucleation under such conditions is much lower than in the presence of SUVs. Despite the lack of observed aggregation, we can define an upper bound for the rate of primary nucleation in the absence of SUVs, by assuming that under these conditions the mechanism of aggregation of α-syn consists of a nucleation step followed by elongation and that the total mass of fibrils varies with time according to 46:

$$M(t)=m(0)[1-(\text{sech}(\sqrt{\frac{n}{2}}\lambda t))^{\frac{2}{n}}] \quad (19)$$

with $\lambda=\sqrt{2k_n k_+ m(0)^n}$. The lowest ThT signal that we measured corresponds to the formation of 4 μM fibrils and is 10 × higher than the signal of the background (Supplementary Fig. 6). We can thus assume that the minimum concentration of fibrils that we can detect using our experimental set up is approximately 0.4 μM, therefore putting an upper bound on the concentration of fibrils formed after 125h. We thus estimated the upper limit of the rate of formation of new nuclei via primary nucleation ($k_n m(0)n$) of α-syn under quiescent conditions using Eq. 19 and the following values for the different constants: M(t) ~ 0.4 μM, $k_+ = 2 \cdot 10^3$ s^{-1}, n = 2 and m(0) = 140 μM and obtained a value of $7 \cdot 10^{-18}$ M s^{-1}. It is worth mentioning, that any contribution from secondary processes, which have been assumed to be negligible in the above equation, would render this value even smaller.

Quiescent conditions in the presence of SUVs—The global analysis of our data sets have shown that in the presence of SUVs, $k_n k_+ = 1.2 \cdot 10^{-5}$ $M^{-(n+1)}$ s^{-2}. For an initial concentrations of α-syn free and α-syn bound to the SUVs of 140 μM and 10 μM, respectively, we can estimate the rate of formation of new nuclei via primary nucleation ($k_n b m(0)^n$) to $1 \cdot 10^{-14}$ M s^{-1}. Under these conditions, the presence of SUVs thus enhanced the rate of formation of new nuclei via primary nucleation of α-syn by a factor of 10^3.

Atomic Force Microscopy

Data Acquisition—For atomic force microscopy (AFM) imaging, samples were diluted to ~1 μM total protein concentration into dH_2O, and 10 μl were pipetted onto freshly cleaved mica (Agar Scientific, Stansted, UK) and left to dry.

The samples were imaged with a Nanowizard II atomic force microscope (JPK Instruments, Waterbeach, UK) in intermittent contact mode in air, using NSC 36 cantilevers (Mikromasch, Tallinn, Estonia) with resonant frequencies between 70 and 150 kHz.

Length distribution analysis—In order to evaluate the number of nucleation sites per vesicle, we estimated the number of fibrils and SUVs in solution by analysing AFM images of the sample taken at the end of the reaction of amyloid formation, when 200 μM α-syn were incubated in the presence of 600 μM DMPS and led to the conversion of 40 μM α-syn into fibrils (Fig. 5a, main manuscript). First, we estimated the concentration of vesicles in solution formed by 600 μM DMPS. We have previously shown (see section" Estimation of the local concentration of α-syn at the surface of a SUV") that there are 6,000 DMPS lipids per SUVs; we thus estimated the concentration of SUVs in solution to 0.1 μM

$$([\mathrm{SUVs}] = \frac{\text{concentration of molecules of DMPS}}{\text{number of molecules of DMPS per SUV}}).$$

Second, the concentration of fibrils in solution was calculated as follows. We estimated the average length of α-syn fibrils by measuring the length distribution of the fibrils on the AFM image (Fig. 5a, main manuscript). The average length of the fibril formed was estimated to be 375 nm which corresponds to ~ 400 monomers per fibril

$$(\frac{\mathrm{length}(\frac{\mathrm{width}}{2})^2 \pi \rho \mathrm{N_A}}{\mathrm{M}},$$ with width = 5 nm, ρ = 1.35 g.cm^{-3} 57, N_A, the number of Avogadro and M, the molecular mass of α-syn). The concentration of fibrils can then be estimated to 0.1 μM $([\mathrm{fibrils}] = \frac{[\alpha - \mathrm{syn}_{\mathrm{fibrils}}]}{\text{number of monomer per fibril}}$, [α-$\mathrm{syn}_{\mathrm{fibrils}}$] = 40 μM), which corresponds to the concentration of SUVs in solution, suggesting that there is of the order of one nucleation event per SUV on average.

Supplementary Material

Refer to Web version on PubMed Central for supplementary material.

Acknowledgements

We wish to thank Myriam Ouberai for her help with the preparation of SUVs and herself, Christopher Waudby and John Christodoulou for valuable discussions. This work was supported by the UK BBSRC (BB/H003843/1, CMD,

MV) and the Wellcome Trust (094425/Z/10/Z, CMD, TPJK, MV), the European Research Council (337969, TPJK) the Frances and Augustus Newman Foundation (TPJK), Magdalene College, Cambridge (AKB), St John's College, Cambridge (TCTM), the Cambridge Home and EU Scholarship Scheme (GM), Elan Pharmaceuticals (CMD, TPJK, MV, CG, AKB) and the Leverhulme Trust (AKB).

References

1. Bellucci A, Navarria L, Zaltieri M, Missale C, Spano P. Alpha-synuclein synaptic pathology and its implications in the development of novel therapeutic approaches to cure Parkinson's disease. Brain Res. 2012; 1432:95–113. [PubMed: 22153624]
2. Bellucci A, et al. From alpha-synuclein to synaptic dysfunctions: new insights into the pathophysiology of Parkinson's disease. Brain Res. 2012; 1476:183–202. [PubMed: 22560500]
3. Chiti F, Dobson CM. Protein misfolding, functional amyloid, and human disease. Annu Rev Biochem. 2006; 75:333–66. [PubMed: 16756495]
4. Dobson CM. Protein misfolding, evolution and disease. Trends Biochem Sci. 1999; 24:329–32. [PubMed: 10470028]
5. Knowles TP, Vendruscolo M, Dobson CM. The amyloid state and its association with protein misfolding diseases. Nat Rev Mol Cell Biol. 2014; 15:384–396. [PubMed: 24854788]
6. Spillantini MG, Goedert M. The alpha-synucleinopathies: Parkinson's disease, dementia with Lewy bodies, and multiple system atrophy. Ann N Y Acad Sci. 2000; 920:16–27. [PubMed: 11193145]
7. Spillantini MG, et al. Alpha-synuclein in Lewy bodies. Nature. 1997; 388:839–40. [PubMed: 9278044]
8. Bodner CR, Dobson CM, Bax A. Multiple tight phospholipid-binding modes of alpha-synuclein revealed by solution NMR spectroscopy. J Mol Biol. 2009; 390:775–90. [PubMed: 19481095]
9. Davidson WS, Jonas A, Clayton DF, George JM. Stabilization of alpha-synuclein secondary structure upon binding to synthetic membranes. J Biol Chem. 1998; 273:9443–9. [PubMed: 9545270]
10. Fusco G, et al. Direct observation of the three regions in alpha-synuclein that determine its membrane-bound behaviour. Nat Commun. 2014; 5:3827. [PubMed: 24871041]
11. Middleton ER, Rhoades E. Effects of curvature and composition on alpha-synuclein binding to lipid vesicles. Biophys J. 2010; 99:2279–88. [PubMed: 20923663]
12. Ouberai MM, et al. Alpha-synuclein senses lipid packing defects and induces lateral expansion of lipids leading to membrane remodeling. J Biol Chem. 2013; 288:20883–95. [PubMed: 23740253]
13. Shvadchak VV, Yushchenko DA, Pievo R, Jovin TM. The mode of alpha-synuclein binding to membranes depends on lipid composition and lipid to protein ratio. FEBS Lett. 2011; 585:3513–9. [PubMed: 22004764]
14. Trexler AJ, Rhoades E. Alpha-synuclein binds large unilamellar vesicles as an extended helix. Biochemistry. 2009; 48:2304–6. [PubMed: 19220042]
15. Abeliovich A, et al. Mice lacking alpha-synuclein display functional deficits in the nigrostriatal dopamine system. Neuron. 2000; 25:239–52. [PubMed: 10707987]
16. Clayton DF, George JM. The synucleins: a family of proteins involved in synaptic function, plasticity, neurodegeneration and disease. Trends Neurosci. 1998; 21:249–54. [PubMed: 9641537]
17. Fortin DL, Nemani VM, Nakamura K, Edwards RH. The behavior of alpha-synuclein in neurons. Mov Disord. 2010; 25(Suppl 1):S21–6. [PubMed: 20187244]
18. Gureviciene I, Gurevicius K, Tanila H. Role of alpha-synuclein in synaptic glutamate release. Neurobiol Dis. 2007; 28:83–9. [PubMed: 17689254]
19. Nemani VM, et al. Increased expression of alpha-synuclein reduces neurotransmitter release by inhibiting synaptic vesicle reclustering after endocytosis. Neuron. 2010; 65:66–79. [PubMed: 20152114]
20. Auluck PK, Caraveo G, Lindquist S. Alpha-synuclein: membrane interactions and toxicity in Parkinson's disease. Annu Rev Cell Dev Biol. 2010; 26:211–33. [PubMed: 20500090]
21. Butterfield SM, Lashuel HA. Amyloidogenic protein-membrane interactions: mechanistic insight from model systems. Angew Chem Int Ed Engl. 2010; 49:5628–54. [PubMed: 20623810]

22. Fink AL. The aggregation and fibrillation of alpha-synuclein. Acc Chem Res. 2006; 39:628–34. [PubMed: 16981679]
23. Giehm L, Svergun DI, Otzen DE, Vestergaard B. Low-resolution structure of a vesicle disrupting alpha-synuclein oligomer that accumulates during fibrillation. Proc Natl Acad Sci U S A. 2011; 108:3246–51. [PubMed: 21300904]
24. Martinez Z, Zhu M, Han S, Fink AL. GM1 specifically interacts with alpha-synuclein and inhibits fibrillation. Biochemistry. 2007; 46:1868–77. [PubMed: 17253773]
25. Zhu M, Fink AL. Lipid binding inhibits alpha-synuclein fibril formation. J Biol Chem. 2003; 278:16873–7. [PubMed: 12621030]
26. Hellstrand E, Nowacka A, Topgaard D, Linse S, Sparr E. Membrane lipid co-aggregation with alpha-synuclein fibrils. PLoS One. 2013; 8:e77235. [PubMed: 24146972]
27. Cohen SI, Vendruscolo M, Dobson CM, Knowles TP. From macroscopic measurements to microscopic mechanisms of protein aggregation. J Mol Biol. 2012; 421:160–71. [PubMed: 22406275]
28. Cohen SI, et al. Nucleated polymerization with secondary pathways. I. Time evolution of the principal moments. J Chem Phys. 2011; 135:065105. [PubMed: 21842954]
29. Knowles TP, et al. An analytical solution to the kinetics of breakable filament assembly. Science. 2009; 326:1533–7. [PubMed: 20007899]
30. Takamori S, et al. Molecular anatomy of a trafficking organelle. Cell. 2006; 127:831–46. [PubMed: 17110340]
31. Dedmon MM, Lindorff-Larsen K, Christodoulou J, Vendruscolo M, Dobson CM. Mapping long-range interactions in alpha-synuclein using spin-label NMR and ensemble molecular dynamics simulations. J Am Chem Soc. 2005; 127:476–7. [PubMed: 15643843]
32. Zhu M, Li J, Fink AL. The association of alpha-synuclein with membranes affects bilayer structure, stability, and fibril formation. J Biol Chem. 2003; 278:40186–97. [PubMed: 12885775]
33. Cabaleiro-Lago C, Quinlan-Pluck F, Lynch I, Dawson KA, Linse S. Dual effect of amino modified polystyrene nanoparticles on amyloid beta protein fibrillation. ACS Chem Neurosci. 2010; 1:279–87. [PubMed: 22778827]
34. Lentz BR. Use of fluorescent probes to monitor molecular order and motions within liposome bilayers. Chem Phys Lipids. 1993; 64:99–116. [PubMed: 8242843]
35. Nuscher B, et al. Alpha-synuclein has a high affinity for packing defects in a bilayer membrane: a thermodynamics study. J Biol Chem. 2004; 279:21966–75. [PubMed: 15028717]
36. Buell AK, et al. Solution conditions determine the relative importance of nucleation and growth processes in alpha-synuclein aggregation. Proc Natl Acad Sci U S A. 2014; 111:7671–6. [PubMed: 24817693]
37. Cohen SI, et al. Proliferation of amyloid-beta42 aggregates occurs through a secondary nucleation mechanism. Proc Natl Acad Sci U S A. 2013; 110:9758–63. [PubMed: 23703910]
38. Meisl G, et al. Differences in nucleation behavior underlie the contrasting aggregation kinetics of the Abeta40 and Abeta42 peptides. Proc Natl Acad Sci U S A. 2014; 111:9384–9. [PubMed: 24938782]
39. Ferrone F. Analysis of protein aggregation kinetics. Methods Enzymol. 1999; 309:256–74. [PubMed: 10507029]
40. Ferrone FA, Hofrichter J, Eaton WA. Kinetics of sickle hemoglobin polymerization. II. A double nucleation mechanism. J Mol Biol. 1985; 183:611–31. [PubMed: 4020873]
41. Oosawa F, Kasai M. A theory of linear and helical aggregations of macromolecules. J Mol Biol. 1962; 4:10–21. [PubMed: 14482095]
42. Xue WF, Homans SW, Radford SE. Systematic analysis of nucleation-dependent polymerization reveals new insights into the mechanism of amyloid self-assembly. Proc Natl Acad Sci U S A. 2008; 105:8926–31. [PubMed: 18579777]
43. Campioni S, et al. The presence of an air-water interface affects formation and elongation of alpha-synuclein fibrils. J Am Chem Soc. 2014; 136:2866–75. [PubMed: 24460028]
44. Giehm L, Lorenzen N, Otzen DE. Assays for alpha-synuclein aggregation. Methods. 2011; 53:295–305. [PubMed: 21163351]

45. Giehm L, Otzen DE. Strategies to increase the reproducibility of protein fibrillization in plate reader assays. Anal Biochem. 2010; 400:270–81. [PubMed: 20149780]
46. Oosawa, F. Thermodynamics of the polymerization of protein. London; New York: Academic Press; 1975.
47. Cremades N, et al. Direct observation of the interconversion of normal and toxic forms of alpha-synuclein. Cell. 2012; 149:1048–59. [PubMed: 22632969]
48. Bishop MF, Ferrone FA. Kinetics of nucleation-controlled polymerization. A perturbation treatment for use with a secondary pathway. Biophys J. 1984; 46:631–44. [PubMed: 6498276]
49. Wilhelm BG, et al. Composition of isolated synaptic boutons reveals the amounts of vesicle trafficking proteins. Science. 2014; 344:1023–8. [PubMed: 24876496]
50. Ciryam P, Tartaglia GG, Morimoto RI, Dobson CM, Vendruscolo M. Widespread aggregation and neurodegenerative diseases are associated with supersaturated proteins. Cell Rep. 2013; 5:781–90. [PubMed: 24183671]
51. Hoyer W, et al. Dependence of alpha-synuclein aggregate morphology on solution conditions. J Mol Biol. 2002; 322:383–93. [PubMed: 12217698]
52. Petrache HI, et al. Structure and fluctuations of charged phosphatidylserine bilayers in the absence of salt. Biophys J. 2004; 86:1574–86. [PubMed: 14990484]
53. Baldwin AJ, et al. Metastability of native proteins and the phenomenon of amyloid formation. J Am Chem Soc. 2011; 133:14160–3. [PubMed: 21650202]
54. Weinreb PH, Zhen W, Poon AW, Conway KA, Lansbury PT Jr. NACP, a protein implicated in Alzheimer's disease and learning, is natively unfolded. Biochemistry. 1996; 35:13709–15. [PubMed: 8901511]
55. Buell AK, et al. Frequency factors in a landscape model of filamentous protein aggregation. Phys Rev Lett. 2010; 104:228101. [PubMed: 20873942]
56. Wales DJ, Doye JPK. Global Optimization by Basin-Hopping and the Lowest Energy Structures of Lennard-Jones Clusters Containing up to 110 Atoms. J Phys Chem A. 1997; 101:5111–5116.
57. Smith JF, Knowles TP, Dobson CM, Macphee CE, Welland ME. Characterization of the nanoscale properties of individual amyloid fibrils. Proc Natl Acad Sci U S A. 2006; 103:15806–11. [PubMed: 17038504]

Europe PMC Funders Author Manuscripts

Europe PMC Funders Author Manuscripts

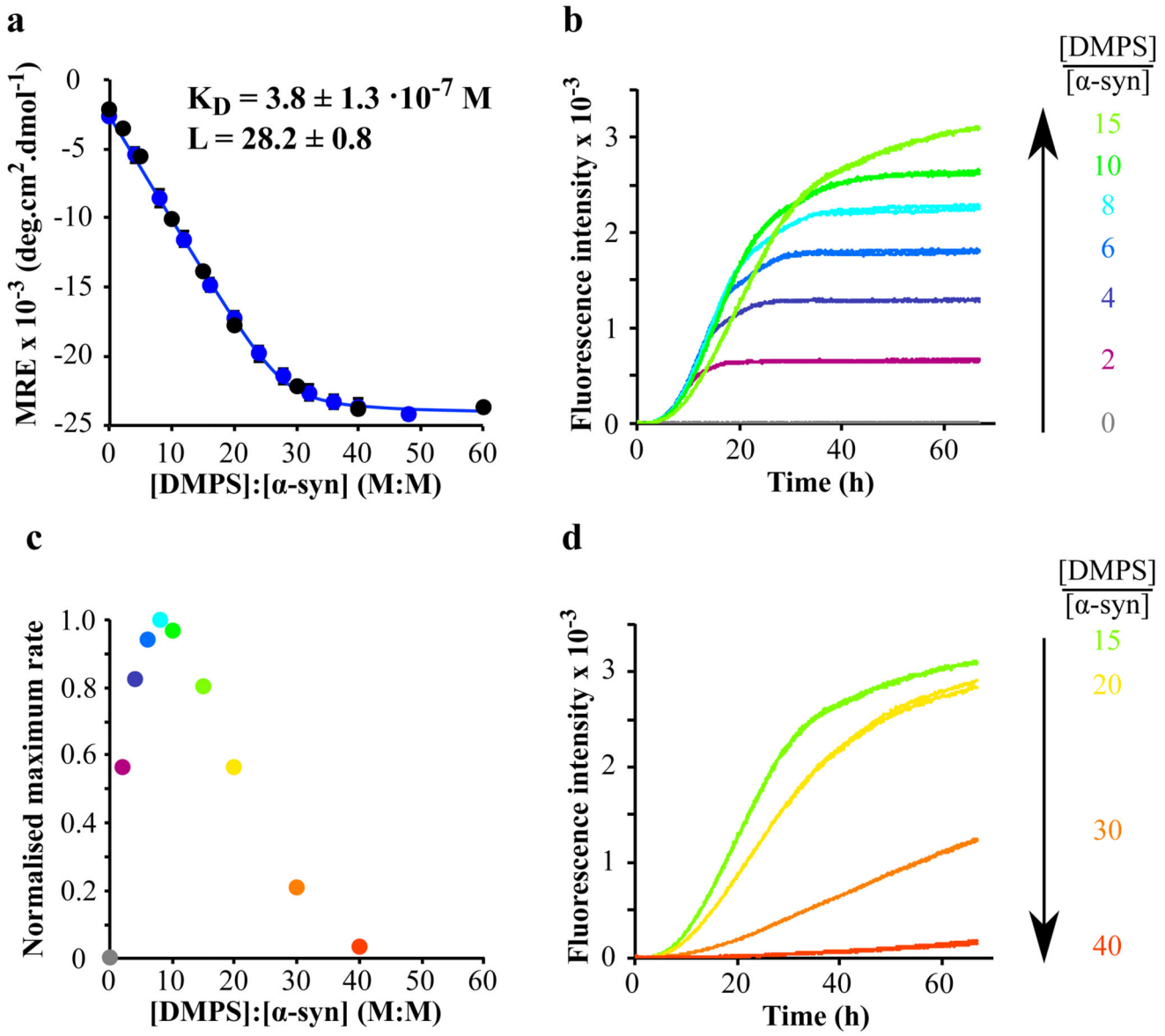

Figure 1. Modulation of the kinetics of α-synuclein amyloid formation by lipid vesicles.

(a) Change in the CD signal of α-syn (25 μM (blue) and 50 μM (black)) measured at 222 nm as a function of [DMPS]:[α-syn] (M:M) ratios. The data (blue dots, 25 μM) fit well to a single step binding model (Eq. 6, $K_D = 3.8 \pm 1.3 \bullet 10^{-7}$ M and L = 28.2 ± 0.8, blue line). L is the stoichiometry of the reaction and corresponds to the average number of lipid molecules bound to each molecule of monomeric α-syn. (b, d) Duplicates of fluorescence measurements monitored as a function of time when α-syn (50 μM) was incubated in the absence (grey) and presence of increasing concentrations of DMPS (100 (purple), 200 (dark blue), 300 (blue), 400 (cyan), 500 (green), 750 (light green), 1000 (yellow), 1500 (orange), 2000 (red) μM). (c) Variation in the maximum rate of aggregation of α-syn with changes in the DMPS: α-syn ratio. For DMPS: α-syn ratios above 40, no stimulation of amyloid formation is observed because effectively all the α-syn monomers required for the growth of

the aggregates are bound to the surfaces of the vesicles. The data correspond to mean values ± s.d.

Europe PMC Funders Author Manuscripts

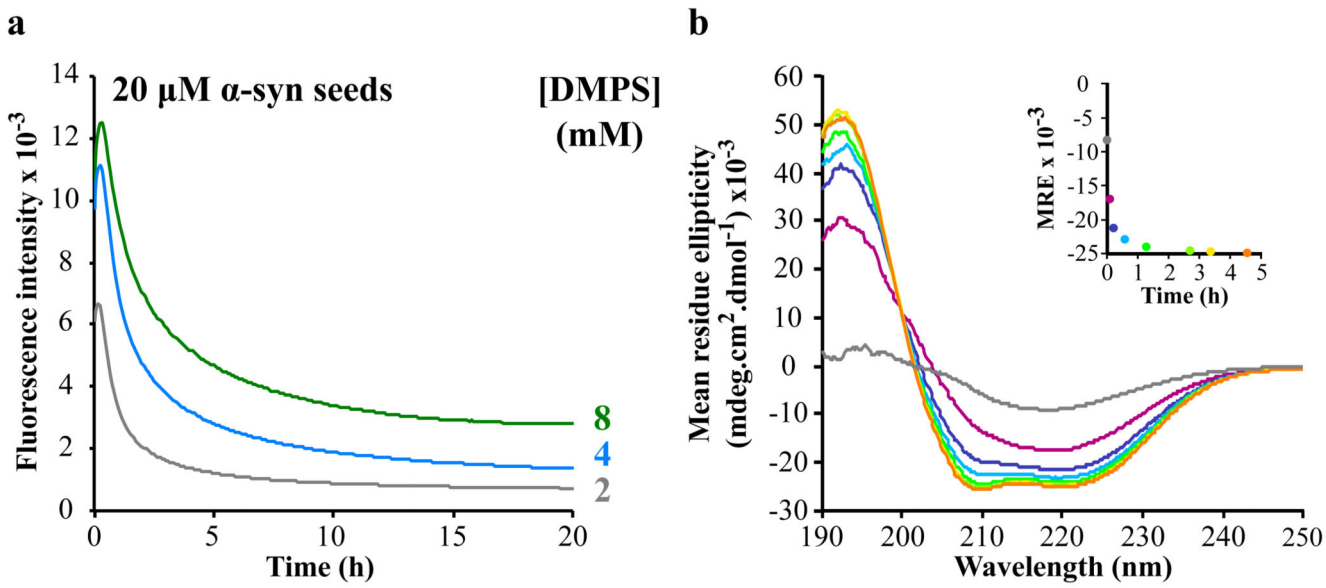

Figure 2. Dissolution of α-syn fibrils in the presence of an excess of DMPS SUVs.

(a) Change in the ThT fluorescence with time when 20 μM pre-formed amyloid fibrils were incubated in the presence of an excess of DMPS SUVs at 37°C (2 mM (grey), 4 mM (blue) and 8 mM (green)). (b) Change in the CD signal of α-syn when 20 μM pre-formed amyloid fibrils were incubated in the presence of 2 mM DMPS SUVs at 37°C (t = 0 (grey), 5 (purple), 17 (dark blue), 39 (blue), 81 (green), 165 (light green), 205 (yellow), 275 min (orange)). Insert: change in the CD signal of α-syn measured at 222 nm as a function of time.

Europe PMC Funders Author Manuscripts

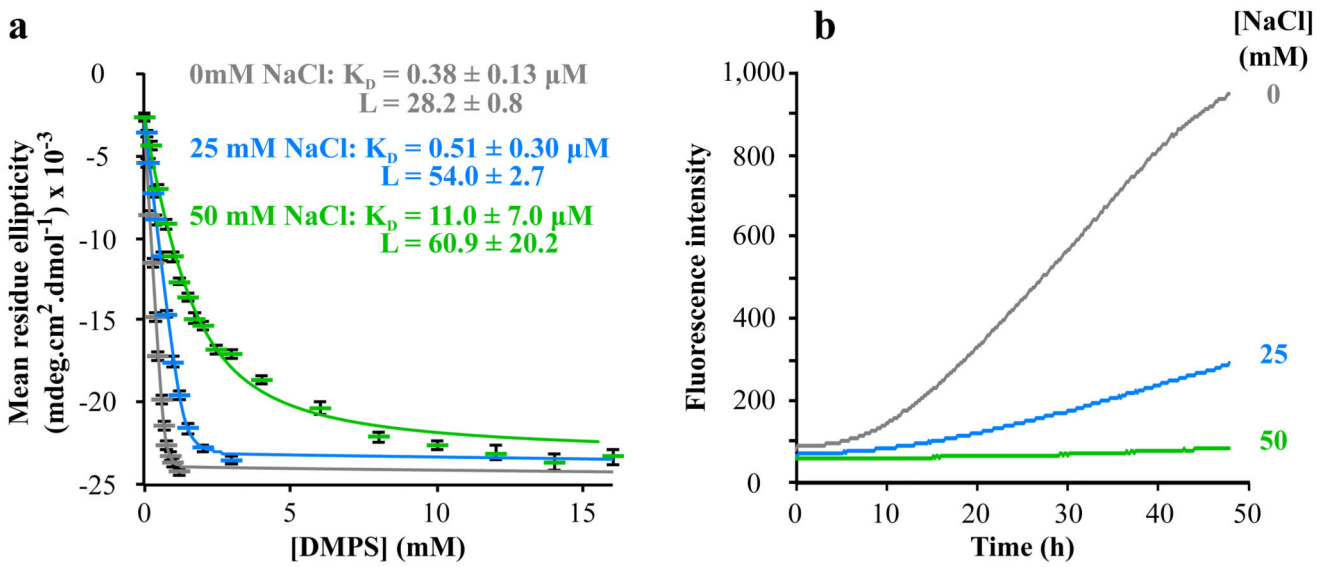

Figure 3. Effect of the presence of salts on the binding of α–syn to DMPS SUVs and on its kinetics of amyloid formation.

(a) Change in the CD signal measured at 222 nm of 50 μM of α-syn monitored in the presence of increasing concentrations of DMPS SUVs in the absence (grey) and the presence of 25 (blue) and 50 mM NaCl (green) at 30°C. (b) Change in the ThT fluorescence when 50 μM α-syn is incubated in the presence of 100 μM DMPS in the absence (grey) and presence of 25 (blue) and 50 mM NaCl (green) at 30°C).

Europe PMC Funders Author Manuscripts

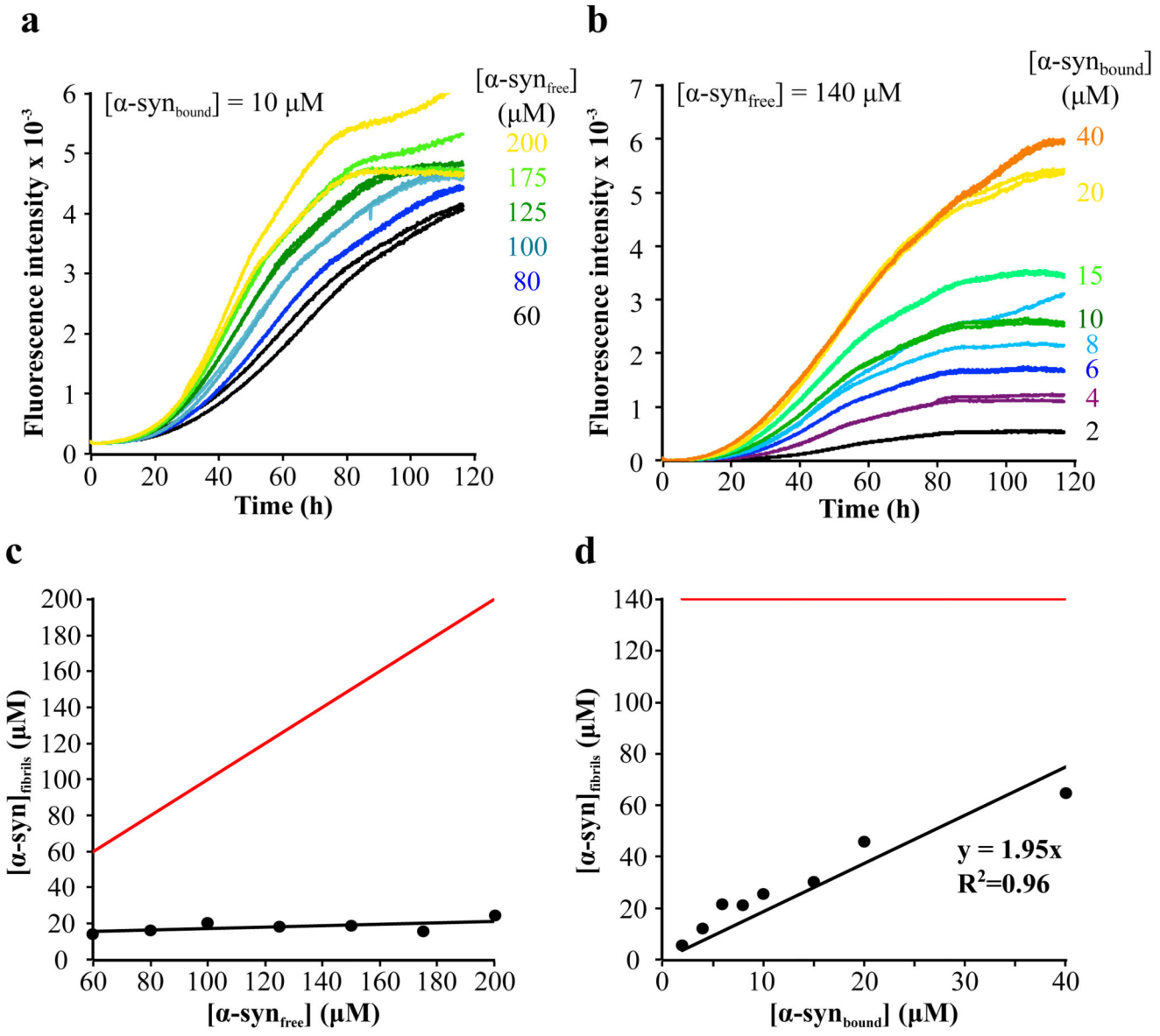

Figure 4. Effect of the variation of the concentration of DMPS SUVs and free monomeric α-syn on the kinetics of α-syn amyloid formation.

(a,b) Duplicates of the change in the fluorescence signal of ThT when increasing concentrations of α-syn (60 (black), 80 (blue), 100 (light blue), 125 (dark green), 175 (green), 200 μM (yellow)) were incubated in the presence of a constant concentration of DMPS (300 μM) (a), and when free monomeric α-syn (140 μM) was incubated in the presence of increasing concentrations of DMPS (60 (black), 120 (purple), 180 (dark blue), 240 (light blue), 300 (dark green), 450 (light green), 600 (yellow), 1200 (orange) μM) (b). (c,d) Change in the concentration of α-syn that is converted into fibrils as a function of the concentration of α-syn free in solution (c), or bound to the SUVs (d). The red lines correspond to the change in the concentration of α-syn that would be converted into fibrils as a function of the concentration of α-syn free in solution (c), or bound to the SUVs (d), if

secondary processes were to dominate the kinetics of α-syn amyloid formation ($[\alpha\text{-syn}_{fibrils}]=[\alpha\text{-syn}_{total}]_{initial}$).

Europe PMC Funders Author Manuscripts

Europe PMC Funders Author Manuscripts

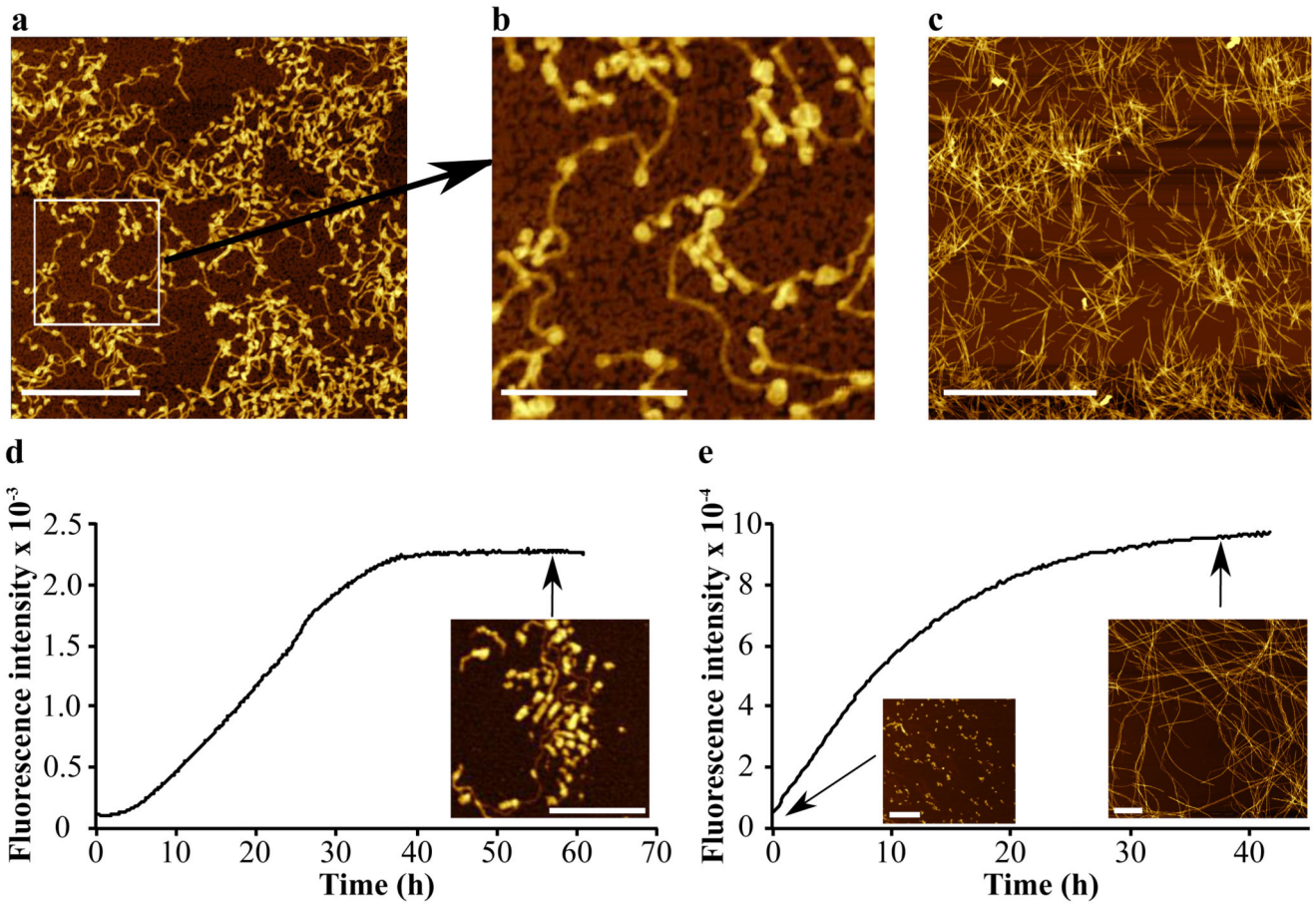

Figure 5. Differences in the morphology of α-syn aggregates formed in the presence and absence of DMPS SUVs.

(a,b) AFM images of aggregates of α-syn formed after incubation of 200 μM monomeric α-syn in the presence of 600 μM DMPS SUVs ((b) Expanded region of the image in (a)) and (c) in the presence of preformed seed fibrils 36. (d, e) Changes in the ThT fluorescence signal observed (d) when the solution of the remaining free monomers is incubated in the presence of fresh DMPS SUVs (300 μM), and (e) after sonication of the reaction mixture for 10s at the end of the process of amyloid formation. The concentrations of α-syn converted into fibrils were found to be 20 (d) and 50 μM (e), respectively. The scale bars of the AFM images correspond to 1 μm (a,e), 500 nm (b,d) and 4 μm (c).

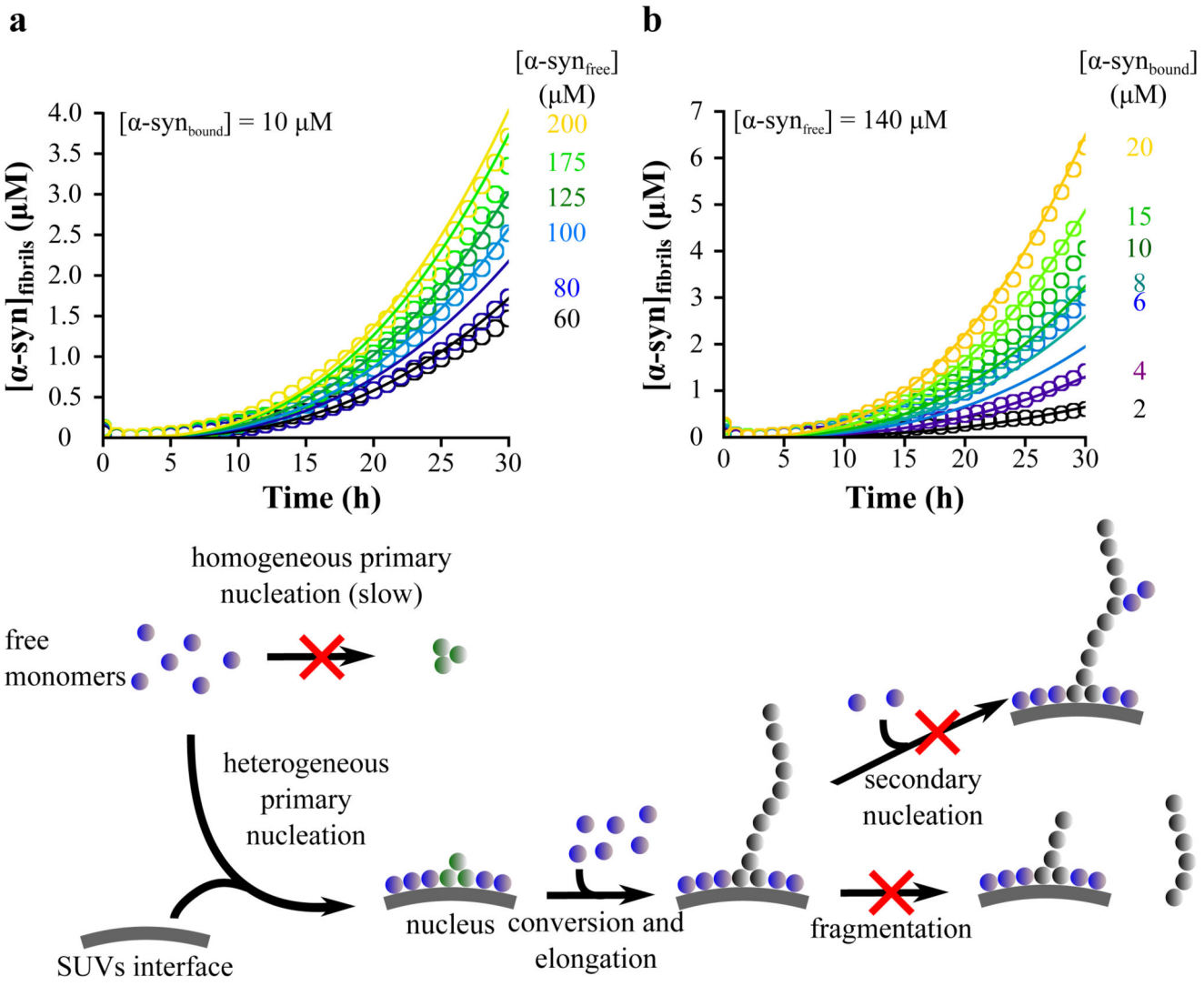

Figure 6. Global kinetic analysis of α-syn aggregation data with a two-step nucleation model.

(a,b) Global fits of the early time-points of the α-syn aggregation curves obtained for the different monomer and DMPS concentrations using a two-step nucleation mechanism (see Methods for details) (Eq. 16, $k_n k_+ = 1.2 \cdot 10^{-5}$ $M^{-(n+1)}$ s^{-2}, $K_M = 125$ μM , $n = 0.2$, $k_b = 1.9 \cdot 10^{-5}$ s^{-1}) (see Fig. 4a,b for the complete time curves). The scheme summarises the proposed mechanism of amyloid formation by α-syn in the presence of DMPS SUVs based on the experimental evidence described in this paper.